Analysis and Optimized Design of Compensation Capacitors for A Megahertz WPT System Using Full-Bridge Rectifier

Minfan Fu, *Member, IEEE*, Zefan Tang, *Member, IEEE*, Chengbin Ma, *Senior Member, IEEE*

***Abstract*—The spatial freedom of wireless power transfer (WPT) systems can be improved using a high operating frequency such as several megahertz (MHz). In the conventional compensations the load of the coupling coils is usually assumed to be pure resistive. However, in MHz WPT systems this assumption is not accurate anymore due to the non-neglectable rectifier input reactance. This paper discusses the impedance characteristics of the full-bridge rectifier at MHz and their influence under the series-series, parallel-series, series-parallel, and parallel-parallel compensation topologies. An undesirable non-zero phase (i.e., none unity power factor) is shown to exist at the primary input port, which leads to decreased power transfer capability. In order to minimize this negative effect, the compensation capacitors are optimally designed, and the series-series topology is found to have the smallest phase under load and coupling variations. Finally, an experimental 6.78 MHz system is built up to verify the optimized design of the compensation capacitors. The results show that the average non-zero phase is effectively reduced together with the improved power factor from 0.916 to 0.982.**

***Index Terms*—Megahertz wireless power transfer, full-bridge rectifier, impedance analysis, compensation capacitors, optimized design**

I. Introduction

WIRELESS power transfer (WPT) has attracted an ever increasing interest over the past few years. It is now being widely applied to charge wearable devices, cellphones, household appliances, and even electric vehicles [1], [2]. These applications have quite different requirements in power level, efficiency, spatial freedom, and size, etc. For charging electronic devices, it is usually desirable to build a WPT system that has a high degree of spatial freedom, and may even be able to simultaneously charge multiple devices [3]–[5]. This requirement can be met by increasing the operating frequency from kilohertz (kHz) to several megahertz (MHz). A higher operating frequency also helps to build more compact and lighter WPT systems.

Various challenges of the MHz WPT systems have been addressed at both circuit and system levels [6]–[9]. Among these existing discussions, one of the most fundamental issues is the analysis and compensation of coupling coils. Four basic compensation topologies, series-series (SS), parallel-series (PS), series-parallel (SP), and parallel-parallel (PP), are well-known and widely used in both kHz and MHz WPT systems. These four topologies have been intensively studied in terms of power transfer capability, efficiency, and output controllability [10]–[13]. Meanwhile, high-order compensation topologies have also been proposed for the WPT applications [14]–[17]. Most of these existing works assume the load of the coupling coils to be pure resistive. This assumption has been verified in kHz WPT applications. However, due to the complex behaviors of the devices such as diodes when working at several MHz, the assumption of a pure resistive load may not be valid anymore. It is because that at MHz, the load of the coupling coils, usually the rectifier input impedance, may contain non-neglectable reactance component. Such undesirable high-frequency characteristics will cause the actual system performance to deviate from the original design target if the conventional analysis and compensation, which is originally developed for kHz WPT applications, are directly applied.

Various topologies of rectifiers have been be proposed for the applications in the MHz WPT. Class E resonant rectifiers were introduced for a high-efficiency rectification at MHz thanks to their soft-switching properties [18]. Another advantage of the Class E rectifiers is the availability of the analytical model. This makes it possible to optimally design the compensation capacitors [19]. However, the high loading sensitivity and high diode voltage stress limit the applications of the Class E rectifiers. Active rectifiers have been developed for small-power (mW) WPT systems in biomedical applications [20], [21]. Meanwhile, they require complicated configurations and drive mechanisms. The full-bridge rectifiers with passive diodes are the most widely used rectifying circuit in electrical systems due to their stable operation and simple topology. Thanks to the development of wide-band-gap devices such as the silicon-carbon (SiC) diodes, high-frequency rectification became achievable when using the full-bridge topology. It is known that in a kHz WPT system, the input impedance of a full-bridge rectifier can be modeled as a pure resistor [22]. However, at several MHz, the diode junction

Manuscript received May 20, 2017; revised March 1, 2018, and April 19, 2018; accepted April 29, 2018. This work was supported by the Shanghai Natural Science Foundation under Grant 16ZR1416300. Paper no. TII-17-1070. *(Corresponding author: Chengbin Ma.)*

M. Fu is with the School of Information Science and Technology, ShanghaiTech University, Shanghai 201210, China (email: fumf@shanghaitech.edu.cn).

Z. Tang is with the Department of Electrical and Computer Engineering, the University of Connecticut, Storrs, CT 06269, USA (email: zefan.tang@uconn.edu).

C. Ma is with the University of Michigan-Shanghai Jiaotong University Joint Institute, Shanghai Jiao Tong University, Shanghai 200240, China (e-mail: chbma@sjtu.edu.cn).

capacitors may resonate with the receiving coil in a WPT system. This makes the rectifier input impedance no longer pure resistive. The impedance characteristics of the full-bridge rectifiers have been partly mentioned in a limited number of published works on WPT. The loading control is developed for a 13.56 MHz WPT system, in which the influence of the input impedance of the full-bridge rectifier is briefly discussed [23]. The improvements are demonstrated by manually tuning the secondary compensation capacitors in a 6.78 MHz system when using a full-bridge rectifier [24].

As to the knowledge of the authors, there lacks intensive analysis on the impedance characteristics of the full-bridge rectifiers when working in MHz WPT systems. This effort is important to improve the design of the compensation and thus the power transfer capability of the overall MHz WPT system. Besides, in real applications variations in the coil relative position (i.e., the coupling) and load are usually common. These uncertainties further add difficulties in optimizing the design of the compensation. This issue has been briefly discussed in [25] for a single compensation topology. This paper is devoted to a comprehensive discussion on the impedance characteristics of the full-bridge rectifier at MHz and their influences under the different compensation topologies. Considering the uncertainties in the load and coupling, a design methodology is further developed to determine the compensation capacitors. It reduces the average non-zero phase of the primary input impedance over the ranges of the coupling and loading variations, and consequentially improves the power transfer capability. Note that the non-zero phase is caused by the reactance component of the input impedance of the full-bridge rectifier when working at MHz. Both the simulation and experiments show that the optimally designed compensation capacitors can significantly reduce the phase of the primary input impedance, and thus improve the power transfer capability and efficiency of the coupling coils.

II. Impedance Analysis

A. System Configuration

A general WPT system is shown in Fig. 1. Power is transferred from the primary side to the secondary side via the two coupling coils, L_p and L_s. k is the coupling coefficient. The compensations on both sides need to be deliberately designed to 1) maximize the power transfer capability on the secondary side, and 2) minimize the volt-ampere (VA) rating on the primary input port. Z_L and R are the rectifier input impedance and final load, respectively.

$$Z_L = R_L + jX_L \text{ and } \theta_L = \tan^{-1}(X_L/R_L), \quad (1)$$

where R_L, X_L, and θ_L are the resistance, reactance, and phase of Z_L, respectively. Similarly, the primary input impendence Z_{IN} is

$$Z_{IN} = R_{IN} + jX_{IN} \text{ and } \theta_{IN} = \tan^{-1}(X_{IN}/R_{IN}). \quad (2)$$

Again, R_{IN}, X_{IN}, and θ_{IN} are the resistance, reactance, and phase of Z_{IN}, respectively.

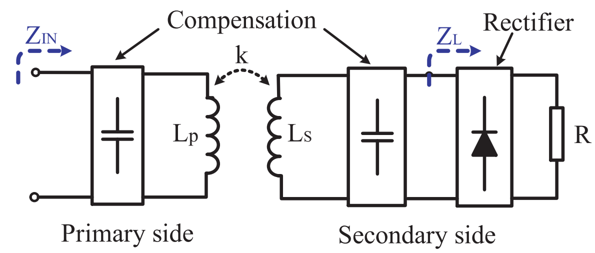

Fig. 1. A general configuration of WPT systems.

B. Rectifier Impedance Characteristics

This paper focuses on the full-bridge rectifiers, which are the most widely used in today's WPT systems including the MHz ones [23]. However, there is a lack of discussion on the behavior of the full-bridge rectifiers and its influence when working in a MHz WPT system. A typical full-bridge rectifier driven by a series compensated receiving coil is shown in Fig. 2. At low frequencies such as within kHz, the switching transition caused by diode junction capacitances (C_1-C_4) is usually neglectable. The input current flows either through D_1-D_4 path or D_2-D_3 path, i.e., the two symmetrical states of the rectifier. However, at MHz, namely with faster switching, the transition due to the junction capacitance becomes significant, as shown in the equivalent circuit and key waveforms in Fig. 3 and Fig. 4. V_L, V_{D1}, and V_{D2} are the voltages of the rectifier input port, D_1, and D_2, respectively; I_L, I_{D1}, I_{C1} and I_{C2} are the currents of the rectifier input port, D_1, C_1, and C_2. Before t_0, D_2 and D_3 are on while the other two diodes are off. When I_L crosses zero and continues to increase, the current cannot commute from D_2-D_3 path to D_1-D_4 path immediately. An additional state happens between t_0 and t_1, as shown in Fig. 3(a). Since all the diodes are off, the input current charges C_2 and C_3 and discharges C_1 and C_4. This resonant state ends when V_{D1} drops to zero, and then the classical state in Fig. 3(b) starts. From t_2 to t_4, the rectifier follows the similar sequence. The overall effect when seeing into the rectifier is that V_L lags I_L, namely $X_L < 0$.

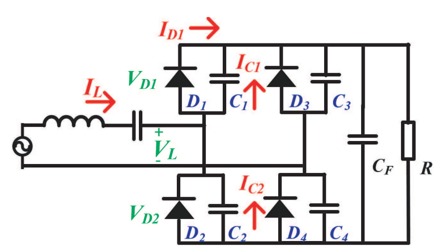

Fig. 2. Circuit diagram of full-bridge rectifier.

According to the previous studies [26]–[28], the diode junction capacitance is usually modeled as a nonlinear function of its reversed bias voltage, namely the C-V curves provided by the manufacturers. The operating frequency and working current are known to have limited influence on the value of the junction capacitance itself. It is challenging to analytically represent Z_L, the input impedance of the full-bridge rectifier, at MHz due to the diode capacitances. Here a well-established radio frequency (RF) simulation software,

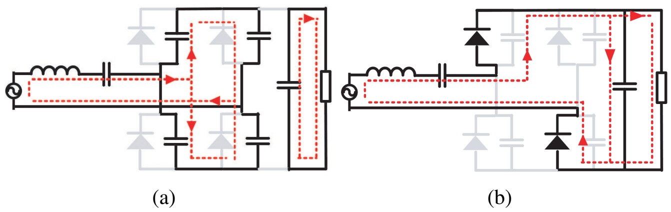

Fig. 3. Equivalent circuits of the operating states for the positive cycle. (a) From t_0 to t_1. (b) From t_1 to t_2.

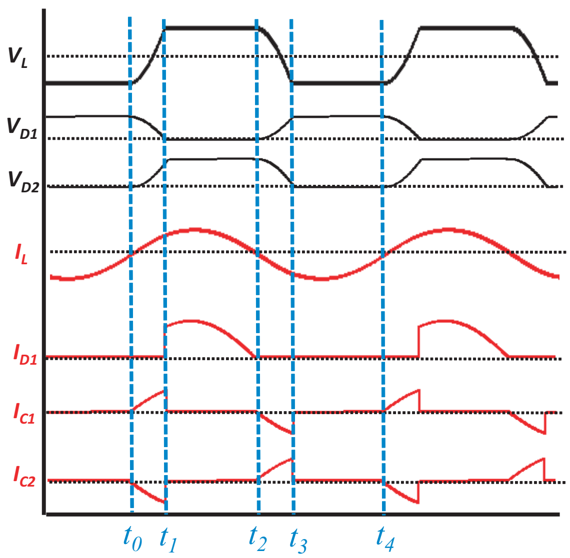

Fig. 4. Key waveforms of the rectifier.

Advanced Design System (ADS) from Keysight Technologies (i.e., Agilent previously), is used to directly give the value of Z_L. For high accuracy, the Pspice model of the diodes, STPSC406, is employed in the simulation. A sinusoidal input current I_L is tuned to achieve a constant output voltage V_R (=10 V) under different final loads, R's.

Fig. 5 compares R_L and θ_L, the resistance component and phase of Z_L, at four different frequencies, 100 kHz, 1 MHz, 6.78 MHz, and 13.56 MHz. Note that at low frequencies such as 100 kHz, R_L is almost linearly proportional to R, and θ_L is almost neglectable. This is because the switching transition is too short and can be ignored [refer to Fig.3 (a)]. Thus in kHz WPT systems, it is a common practice to represent Z_L as a pure resistor [22],

$$Z_L = R_L = \frac{8R}{\pi^2}. \tag{3}$$

However, a higher operating frequency leads to a more nonlinear curve of R_L versus R. The phase θ_L also becomes much more obvious. Since the transition time become comparable to the switching period, it leads to a capacitive Z_L, i.e., a negative θ_L. In addition, at a specific frequency, a larger R lowers the capacitor charging/discharging current and increases length of the transition time. Therefore, a larger negative θ_L is observed. Generally speaking, simply modeling Z_L as a pure resistor is no longer sufficient for the applications in MHz WPT.

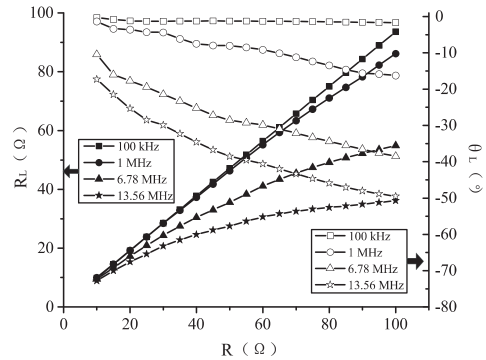

Fig. 5. Rectifier input impedance at different frequencies.

At MHz, the negative θ_L is caused by the diode junction capacitance, which is affected by the reversed bias voltage. Thus the required rectifier output voltage V_R influences the rectifier input impedance, Z_L. Different applications may have different constant V_R's. Fig. 6 shows the influence of V_R over Z_L. Since the junction capacitance decreases with an increasing bias voltage, higher V_R results in smaller θ_L. Meanwhile, another factor that affects the input impedance characteristics is the diode itself. As shown in Fig. 7, another type of diode (Infineon: IDK04G65C5) is compared with the above selected diode (ST Microelectronics: STPSC406), in terms of Z_L for the 6.78 MHz rectification. Although the exact values are slightly different, the same conclusion can be drawn from the comparison, namely the need of compensating the capacitive Z_L.

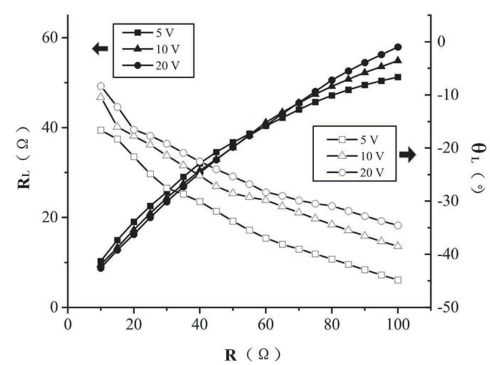

Fig. 6. Rectifier input impedance under different V_R

.

The secondary compensation, i.e., the driving source of the rectifier, also affects Z_L. As shown in Fig. 8, series or parallel compensation can be applied to form different resonant circuits. Although the induced voltage V_s is the same for both cases, the direct driving source (V_L and I_L) of the rectifier is quite different. For the series compensation, the rectifier is driven by a sinusoidal current source, and the load of the rectifier must be a voltage sink. However, the load of the rectifier should be a current sink if parallel compensation is applied. Fig. 9 shows the rectifier input impedance under different secondary compensations (L_s is 3.34 μH, and C_s resonates with L_s at 6.78 MHz). Compared with Z_L under

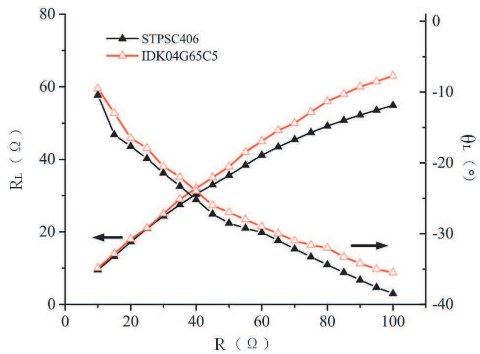

Fig. 7. Rectifier input impedances when using different diodes at 6.78 MHz.

the series compensation, Z_L under the parallel compensation has obviously larger R_L and θ_L.

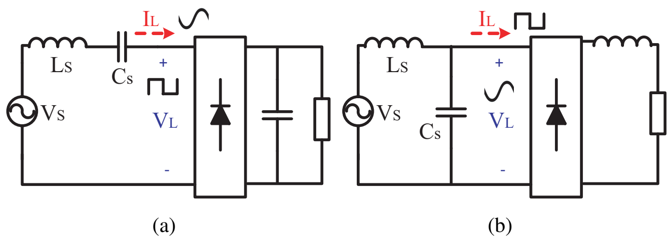

Fig. 8. Two basic secondary compensations. (a) Series compensation. (b) Parallel compensation.

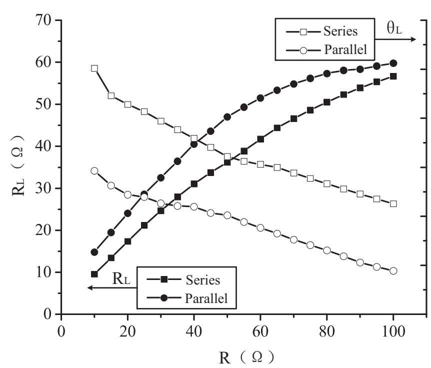

Fig. 9. Z_L at 6.78 MHz and under secondary series/parallel compensations.

C. Influence of Rectifier Input Impedance

In a WPT system, compensations are required on both sides for a maximized power transfer capability. The four basic compensation topologies, SS, PS, SP, and PP, are widely used thanks to their simple structures. As shown in Fig. 10, C_s forms a resonant circuit with L_s to boost the power transfer capability, and C_p should also be deliberately designed to reduce the VA rating at the primary input port. Ideally, this can be achieved by letting

$$\omega L_s - \frac{1}{\omega C_s} = 0 \quad \text{and} \quad X_{IN} = 0, \tag{4}$$

where ω is the resonance frequency and X_{IN} is the reactance component of Z_{IN}, the primary input impedance. In the conventional analysis for the kHz WPT systems, Z_L is usually assumed to be pure resistive, i.e., a neglectable X_L. Thus for the different compensation topologies,

$$C_s = \frac{1}{\omega^2 L_s}, \tag{5}$$

which is constant with a given L_s. The required C_p has already been derived to achieve a zero X_{IN}, as summarized in Table I [10].

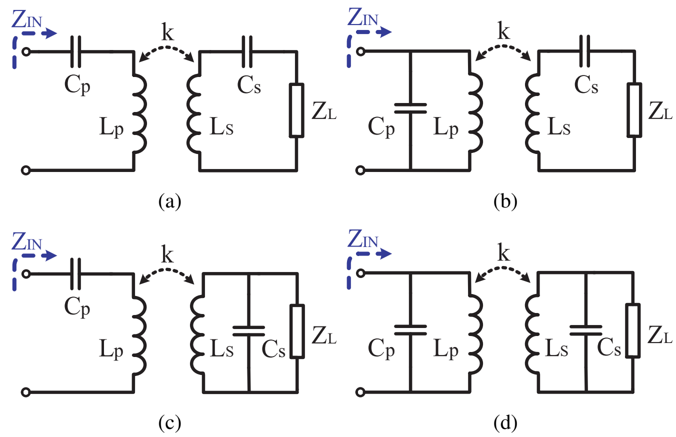

Fig. 10. Four basic compensation topologies. (a) SS. (b) PS. (c) SP. (d) PP.

TABLE I
REQUIRED C_p ASSUMING A ZERO X_L.

SS	$\frac{1}{\omega^2 L_p}$
PS	$\frac{1}{\omega^2 L_p(1+\omega^2 L_s^2 k^4/R_L^2)}$
SP	$\frac{1}{\omega^2 L_p(1-k^2)}$
PP	$\frac{(1-k^2)}{\omega^2 L_p(1-k^2)^2+k^4 L_p R_L^2/L_s^2}$

However, as discussed above, X_L becomes non-neglectable when working at MHz. This obvious X_L leads to a non-zero X_{IN} if the conventional compensations listed in Table I are directly applied. Theoretically these conventional compensations can be modified to completely cancel the influence of the non-zero X_L. Again (4) and (5) are used to derive the required C_s and C_p. The modified C_p's are newly calculated and listed in Table II. All the C_p's now contain new terms relating to X_L. Letting X_L=0, they are equivalent with the previous results in Table I. Table II shows that all the C_p's depend specific values of Z_L and k. Ideally it requires a variable C_p. This property is undesirable for real WPT systems, which usually work in a dynamic environment such as with variations in load (i.e., Z_L) or coupling (i.e., coil relative position and thus k). Similarly, C_s can be tuned targeting a specific Z_L, but again the fixed C_s fails to correspond to the cases with variations in the load and coupling. Although dynamic impedance matching networks can be possibly applied, they may introduce additional power losses as well as added space and weight. For WPT systems working at kHz, the operating frequency itself provides another degree of control freedom to eliminate the phase deviation. However, because of the narrow ISM (industrial, scientific, and medical) bands, this frequency modulation is not implementable in MHz WPT applications [29]. Usually in practice, a static compensation is more attractive, particularly for small-size low/medium-power MHz WPT systems. This aspect and the solution are further discussed in the following section.

TABLE II
MODIFIED C_p WITH NONZERO X_L.

SS	$\frac{1}{\omega^2 L_p - \omega^3 k^2 L_p L_s X_L/(R_L^2+X_L^2)}$
PS	$\frac{R_L^2+X_L^2-\omega k^2 L_s X_L}{\omega^2 L_p(\omega^2 k^4 L_s^2+R_L^2+X_L^2-2\omega k^2 L_s X_L)}$
SP	$\frac{1}{\omega^2 L_p(1-k^2)+\omega^2 k^2 L_p X_L/L_s}$
PP	$\frac{L_s^2(1-k^2)+k^2 X_L L_s/\omega}{\omega^2 L_p L_s^2(1-k^2)^2+k^4 L_p R_L^2+k^2 X_L L_p(k^2 X_L+2\omega L_s-2k^2\omega L_s)}$

III. OPTIMIZED DESIGN

A. Design Procedure

All the four basic compensation topologies, SS, PS, SP, and PP, can provide two degrees of design freedom, the values of the two compensation capacitors, C_p and C_s. The purpose of the optimized design is to determine a set of C_p and C_s that minimizes the reactance component (i.e., the phase) of the primary input impedance, Z_{IN}, over wide ranges of the coil coupling (k) and load (R). This effort improves the robustness of a final MHz WPT system, particularly the power transfer capability, when changes occur in the coil relative position and load. Here an index σ is defined to represent the average absolute value of the phase of the primary input impedance, $|\theta_{IN}|$, over ranges of k and R,

$$\sigma = \frac{\sum_{n=0}^{N_k}\sum_{m=0}^{N_R}|\theta_{IN}(C_p, C_s, k, R)|}{(N_k+1)(N_R+1)}, \tag{6}$$

where

$$\begin{cases} k = k_{\min} + n \times \Delta k \\ R = R_{\min} + m \times \Delta R \\ N_k = (k_{max} - k_{min})/\Delta k \\ N_R = (R_{max} - R_{min})/\Delta R \end{cases}. \tag{7}$$

The ranges of k and R are within $[k_{min}, k_{max}]$ and $[R_{min}, R_{max}]$, respectively; N_k and N_R are the total numbers of sampling instants, n and m, for k and R; Δk and ΔR are the sampling steps.

Thus the design optimization is formulated to minimize σ when k and R vary, in which C_p and C_s are the design parameters, and k and R are the variables,

$$\min_{C_p,\ C_s} \quad \sigma(C_p, C_s, k, R) \tag{8}$$

$$s.t. \quad k_{min} \le k \le k_{max}, \tag{9}$$

$$R_{min} \le R \le R_{max}. \tag{10}$$

In the optimization,

1) The coupling coils are represented using their respective analytical models in the four compensation topologies;
2) For the full-bridge rectifier, it is known to be difficult to analytically express Z_L, its input impedance, as a function of R when working at MHz. Lookup tables are generated to represent the relationship through the high-accuracy ADS-based simulation or experimental measurements (see Figs. 5 and 18);
3) The numerical model of the overall MHz WPT system is built using the lookup tables and the analytical models of the coils.

In considering the nature of the above optimization problem, the well-known genetic algorithm (GA), a population-based natural selection approach, can be applied to locate a global or near-to-global optimal set of C_p and C_s [30]. Note that the GA itself is known as unable to guarantee the convergence. The final solution aims at minimizing σ in (8), the average deviation of θ_{IN} from zero, over the specified ranges of k and R in (9) and (10). This solution can be conveniently verified later through the ADS-based simulation. For reference purposes, the program flow chart is shown in Fig. 11.

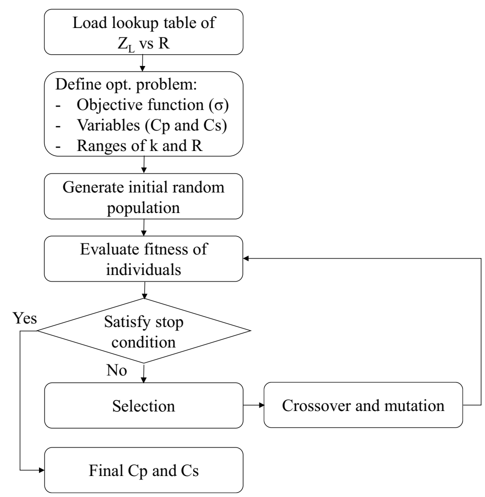

Fig. 11. Program flow chart of the GA-based optimization.

B. Fixed Coupling and Varying Load

The compensation capacitors, C_p and C_s, are first optimized for an example 6.78 MHz WPT system assuming a fixed k. The final load, R, varies between 10 and 100 Ω. The system parameters are given in Table III. The capacitors of the four basic topologies are optimized following the above design procedure and under a condition of a constant output voltage, V_R (=10 V). The two capacitors in the conventional design are calculated using (5) and Table I. Note that in PS and PP topologies C_p depends on the value of R_L (see Table I). Here a medium 50 Ω R_L is assumed in the conventional design.

TABLE III
SYSTEM PARAMETERS

Frequency	L_p, L_s	R_{min}	R_{max}	ΔR	k	V_R
6.78 MHz	3.34 μH	10 Ω	100 Ω	1 Ω	0.15	10 V

TABLE IV
DESIGNS OF COMPENSATIONS UNDER A FIXED COUPLING.

		Cp (pF)	Cs (pF)	$\sigma(^\circ)$	R_{IN} (Ω)
SS	Conventional	165	165	27.1	[5.1, 46]
	Optimized	160	168	2.0	[5.3, 47]
PS	Conventional	164	165	27.7	[4.5E^2, 2.8E^3]
	Optimized	160	172	5.4	[4.3E^2, 3.8E^3]
SP	Conventional	169	165	41.6	[0.33, 1.4]
	Optimized	170	145	20.4	[0.33, 1.6]
PP	Conventional	169	165	47.4	[5.0E^3, 3.6E^4]
	Optimized	170	154	23.2	[8.7E^3, 2.0E^4]

The results using the conventional and optimized compensations are compared in Table IV and Fig. 12(a)–(d). Under the conventional compensations, all the topologies show a significant phase deviation, i.e., σ's between 27.1–47.4°, while through the optimized design, the deviations are largely reduced, 2.0–23.2°. It can be seen that the secondary side using the series compensation, namely SS or PS, achieves a much smaller σ than that using the parallel compensation, SP or PP. Another important result is the value of R_{IN}, which is especially large in PS and PP topologies. This requires a high driving voltage to transfer sufficient amount of power. The SS topology is generally suitable for the present MHz WPT system.

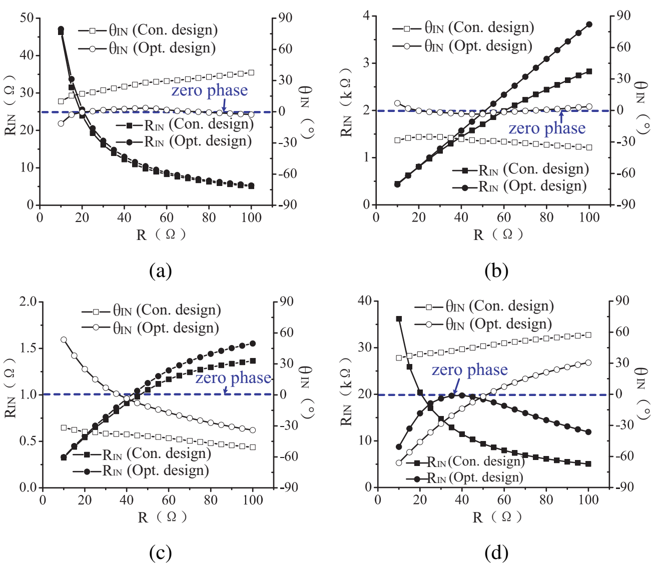

Fig. 12. R_{IN} and θ_{IN} using the conventional and optimized designs. (a) SS. (b) PS. (c) SP. (d) PP.

C. Varying Coupling and Load

The SS topology, which is expected to have a small σ and reasonable range of R_{IN}, is further investigated when k (i.e., the coil relative position) varies between 0.1 and 0.2. The GA-based optimization uses the parameters in Table III and $\Delta k = 0.01$. The results of the optimization are summarized in Table V. It shows that the phase deviation is significantly reduced, from 27.1° to 9.2°, by employing the optimally designed compensation capacitors. However, the variation in k leads to a larger achievable σ (=9.2°) in Table V compared to that of the SS topology, 2.0°, in Table IV.

TABLE V
DESIGNS OF COMPENSATIONS UNDER A VARYING COUPLING.

		Cp (pF)	Cs (pF)	$\sigma(^\circ)$	R_{IN} (Ω)
SS	Conventional	165	165	27.1	[2.3, 82]
	Optimized	162	169	9.2	[2.4, 82]

For reference purposes, θ_{IN} and R_{IN} under various k and R are shown in Fig. 13(a) and (b), respectively. The curves of θ_{IN} overlap when the conventional compensation is applied. It is because that the conventional SS compensation reverses the phase, i.e., $\theta_{IN} = -\theta_L$, and this property is independent from k. Thus using the conventional compensation, σ (=27.1°) under the varying k is as same as the one under the fixed k. From Fig. 13(b), it can be seen that both the two SS compensations have a similar influence on R_{IN}.

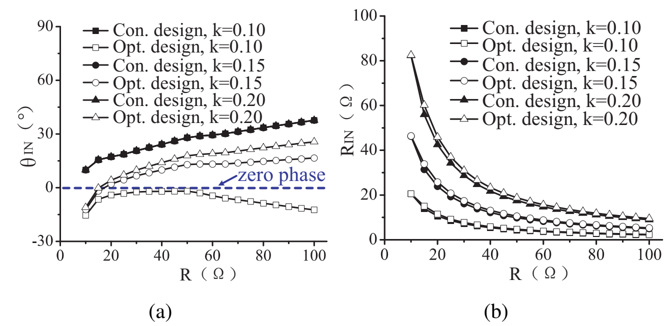

Fig. 13. θ_{IN} and R_{IN} under different k and R. (a) θ_{IN}. (b) R_{IN}.

D. On Variations in Parasitic Resistance and Capacitance

MHz WPT systems enable compact coupling coils that can be fabricated using print circuit boards (PCBs). Compared with the coils being made of liz wire in kHz systems, the PCB-based coils are easy to control the variation in their parasitic resistances and suitable for mass production. In MHz systems, high-quality-factor (>2000) and low-tolerance ($\pm1\%$ variation) ceramic capacitors can be used for compensation. In the present MHz system, the influences of variations in the coil parasitic resistances (ESRs) and capacitances are investigated and shown in Fig. 14. Three cases are compared taking the case of $k = 0.15$ in Fig. 13 as an example. Fig. 14 validates that both the coil ESR and capacitance variations have quite limited influences on the final optimization results.

IV. EXPERIMENTAL VERIFICATION

A. Experimental Setup

As shown in Fig. 15, a 6.78 MHz WPT system is built up for verification purposes. It consists of a commercial Class A power amplifier (PA), two series compensated coils (i.e., the SS compensation), a full-bridge rectifier (diode: STPSC406), and an electronic load. The Class A PA can amplify a small sinusoidal signal with high linearity and thus act as a pure

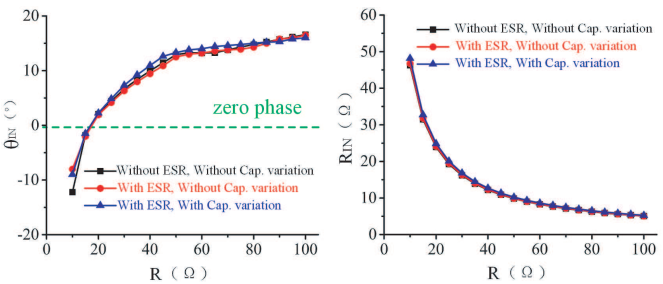

Fig. 14. Influences of coil ESR (=0.7 Ω) and capacitance variations (+1%). (a) θ_{IN}. (b) R_{IN}.

sinusoidal voltage source. Since it works at the linear region of the switch, the PA's efficiency is below 50%. The above commercial PA provides interface to manually adjust its output power to maintain constant V_R (=10V). Thus it is convenient to experimentally investigate the power transfer capability of the MHz WPT system. Note that in practice another switched-mode PA, such as Class D PA or Class E PA, can be possibly applied to improve the PA efficiency [8]. Two identical coupling coils are placed face to face with a vertical distance d (see Fig. 15(b)). In the experiments, d is changed from 25 to 45 mm that corresponds to k between 0.11 and 0.21. This example variation range of the transfer distance and thus that of the coupling coefficient are selected for verification purposes. The electronic load is manually adjusted to emulate different final load, R. The experimental parameters are given in Table VI. Multiple high-Q ceramic capacitors (quality factor $Q_C > 2000$) can be connected in parallel to realize the required capacitance. The parameter Q_L is the qualify factor of the coils. The voltage and current at different ports are measured using the oscilloscope for the following impedance calculation. In real applications, a dc/dc converter or a battery could be connected after the rectifier. For either case, the proposed design methodology is still valid through extracting the specific variation range of the equivalent load resistance seen by the rectifier.

TABLE VI
EXPERIMENTAL PARAMETERS.

k_{min}	k_{max}	Δk	R_{min}	R_{max}	ΔR
0.11	0.21	0.05	10 Ω	100 Ω	10 Ω
V_R	L_p	L_s	Q_L	Q_C	Diode
10 V	3.34 μH	3.34 μH	200	> 2000	STPSC406

B. Conventional Design

The rectifier input impedance, Z_L, is first measured under the conventional compensation, where both C_p and C_s are 165 pF [refer to Table V]. The example waveforms of the rectifier input voltage V_L and current I_L are shown in Fig. 16 when $R = 50\ \Omega$. For the current-driven full-bridge rectifiers working at low frequencies such as kHz, sinusoidal I_L and square V_L should be observed with a neglectable phase difference. However, the actual waveforms in Fig. 16 show that at 6.78

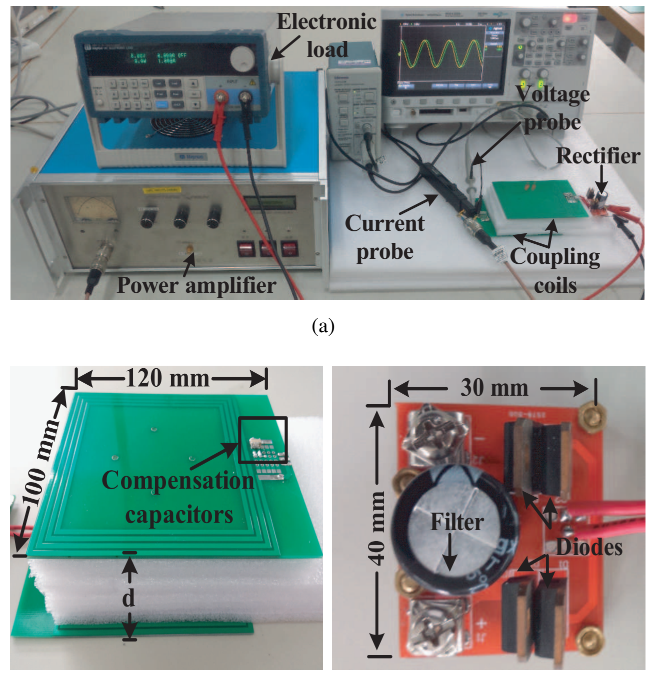

(a)

(b) (c)

Fig. 15. Experimental setup. (a) Overview. (b) Coupling coils. (c) Full-bridge rectifier.

MHz, V_L obviously lags behind I_L (θ_L=$-27°$). This verifies the existence of the negative X_L. The voltage oscillations are mainly caused by the resonance between the lead inductance and junction capacitance. The conduction state in Fig. 3(b) is modified to explain the high-frequency oscillation. Without lead inductance, D_2 and D_3 are reversely blocked and the voltages across C_2 and C_3 should be square waves, as shown in Fig. 4. Fig. 17 shows the oscillation paths when considering the lead inductances, i.e, L_{1-4}. Since the oscillation frequency is higher than the coil resonance frequency, L_sC_s tank acts as an open circuit, while C_F acts as a short circuit. The final waveform in Fig. 16(a) is formed by the combination of the oscillating voltage and square-wave voltage. In the low-frequency kHz WPT systems, this oscillation also exists. But it is not obvious because the switching period is much longer than the oscillation period.

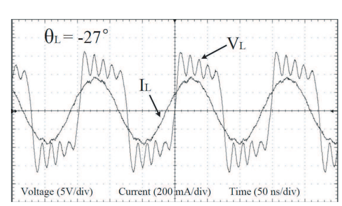

Freq. (MHz)	Resistance (Ω)	Phase (deg.)
6.78	36	-30
13.56	0.33	-89.92
20.34	0.28	-89.95
27.12	0.26	-89.97
33.90	0.25	-89.98

(a) (b)

Fig. 16. Impedance measurement and calculation. (a) Rectifier input voltage and current waveforms when $R = 50\ \Omega$. (b) Results of Fourier transformation.

The measured waveforms can then be used to calculate the impedance through Fourier transformation. The calculation results from the waveforms in Fig. 16(a) are given in Fig. 16(b). It shows that the rectifier almost behaves as a capacitor at harmonic frequencies. At the same time, due to the series

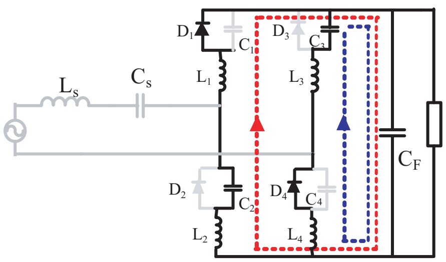

Fig. 17. High-frequency oscillation paths when considering the lead inductances.

resonance between L_S and C_S, I_L is almost pure sinusoidal. Therefore, there is a very limited amount of harmonic energy being transferred. The optimized compensation here focuses on improving the power transfer capability at the fundamental frequency. Similarly, the waveforms for the other R's are measured to calculate the corresponding Z_L's. The measured R_L and θ_L are shown in Fig. 18 under different R. The results are consistent with the simulated curves of the series compensation in Fig. 9.

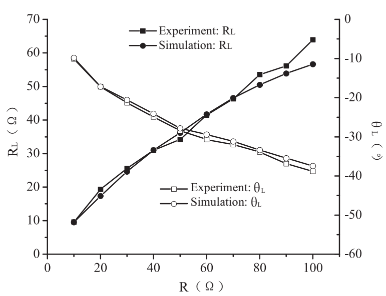

Fig. 18. Measured and simulated R_L and θ_L under the SS topology.

TABLE VII
COMPENSATIONS UNDER A VARYING COUPLING IN EXPERIMENTS.

		Cp (pF)	Cs (pF)	$\sigma(°)$	R_{IN} (Ω)
SS	Conventional	165	165	23.6	[3.5, 89]
	Optimized	161	168	10.8	[3.6, 95]

C. Optimized Design

Here the two compensation capacitors, C_p and C_s, are optimized following the design procedure developed in section III-A. The measured relationship between Z_L and R in Fig. 18 is used to build the lookup table of the full-bridge rectifier. The values of the two capacitors, average phase deviation σ, and primary input resistance R_{IN} are shown and compared in Table VII when using the conventional and optimized designs. Note that in the optimized design, C_p and C_s are calculated assuming a varying k from 0.11 and 0.21.

The waveforms of the primary input voltage V_{IN} and current I_{IN} are shown in Fig. 19 when R=50 Ω. With the conventional design (i.e, the left subfigures), obvious phase deviations are observed due to the capacitive Z_L. Using the optimally designed compensation, the phase deviations are significantly reduced, as shown in the right subfigures. Similar waveforms are obtained for the other loads, and used to calculate θ_{IN} and R_{IN} in Fig. 20. The figure shows that the optimized compensation can effectively suppress the deviation of θ_{IN} from zero. The average phase deviation is reduced from 23.6° to 10.8°, which corresponds to the improved power factor, i.e., cos(θ_{IN}), from 0.916 to 0.982. Unlike the simulation results, the curves of θ_{IN} under the conventional compensations do not completely overlap with each other in experiments [refer to Fig. 13 (a)]. It is mostly due to the parasitic resistances of the coils. Again, as shown in Fig. 20(b), both the conventional and optimized compensations have similar R_{IN}'s despite different k. All the experimental results well match the simulated ones in Fig. 13.

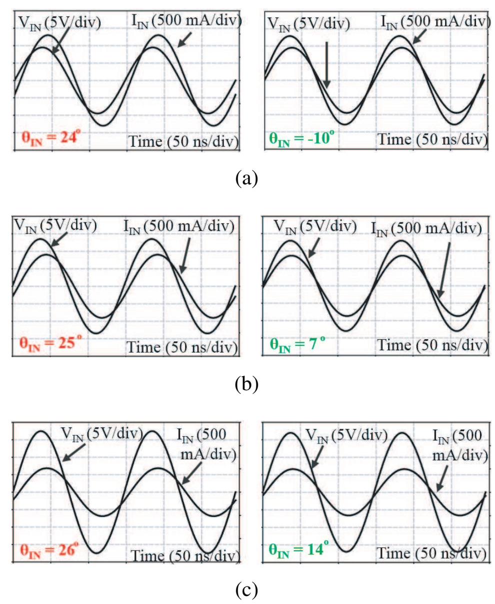

Fig. 19. Voltage and current waveforms at the primary input port when R=50 Ω (left: conventional design; right: optimized design). (a) $k = 0.11$, $d = 45mm$. (b) $k = 0.16$, $d = 30mm$. (c) $k = 0.21$, $d = 25mm$.

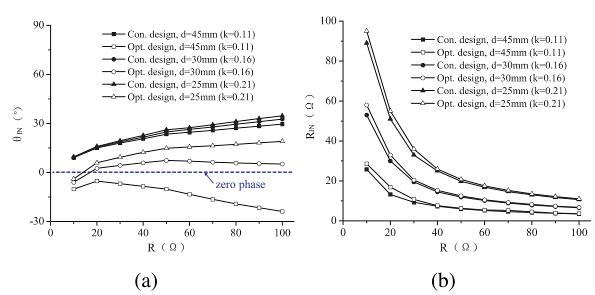

Fig. 20. Measured θ_{IN} and R_{IN} under different k. (a) θ_{IN}. (b) R_{IN}.

It should be noted that the reduced phase helps to improve the power transfer capability as well as the coil efficiency. Here the coil efficiency is defined as the power entering the rectifier over the power entering the primary side, namely without including the rectifier efficiency. For the coupling coils, only the conduction losses exist due to the ESRs of L_p, L_s, C_p, and C_s. For such resonant networks, the quality factors of the components are a direct measure of the efficiency. As shown in Table VI, the quality factors of the capacitors ($Q_C > 2000$) are much higher than those of the coils ($Q_L = 200$). Thus Q_L plays a dominate role in the coil efficiency. In the resonant tanks, an improved power factor leads to a smaller input current when transferring the same amount of power under the same input voltage. It reduces conduction losses and in turn improves the coil efficiency, as shown in Fig. 21.

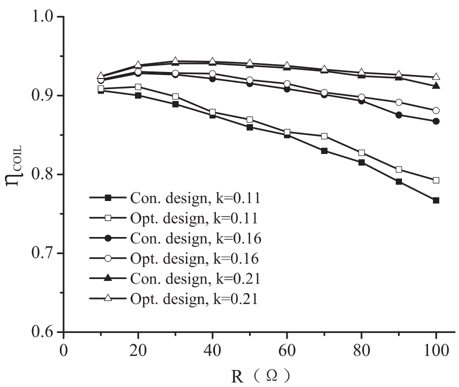

Fig. 21. Measured coil efficiencies (η_{coil}) under different k.

It should be especially noted that the MHz WPT is a candidate technology for loosely coupled systems, i.e., with long transfer distance and low coupling coefficient. Fig. 22 shows the experimental results with even lower coupling coefficients (k=0.11, 0.08, and 0.05), which correspond to transfer distances from 45 mm to 70 mm. Again the capacitors, C_p and C_s, are optimized using the proposed approach. Similar to Fig. 20, the average phase deviation is reduced from 21.7° to 9.4°, namely an improved power factor from 0.929 to 0.986.

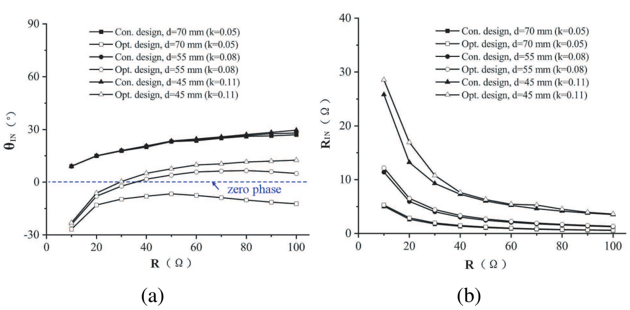

Fig. 22. Measured θ_{IN} and R_{IN} under even lower k's. (a) θ_{IN}. (b) R_{IN}.

V. Conclusion

This paper systematically discusses the influence of the impedance characteristics of the full-bridge rectifier at MHz under different compensation topologies, SS, SP, PS, and PP. With the non-zero rectifier reactance, an undesirable non-zero phase at the primary input port is shown and explained when applying the conventional compensations. In order to minimize this non-zero phase over ranges of the load and coupling, a design approach is proposed to optimize the primary and secondary compensation capacitors. In terms of minimizing the average phase deviation and providing a proper range of the primary input resistance, the SS topology is shown to be an attractive one for the discussed 6.78 MHz WPT system. In the final experiments, the load and coupling coefficient vary between [10, 100] Ω and [0.11, 0.21], respectively. The results show that the optimally designed SS compensation can increase the power factor from 0.916 to 0.982. This effort helps to improve the power transfer capability of the MHz WPT system, and also contributes to an enhanced coil efficiency.

References

[1] H. H. Wu, A. Gilchrist, K. D. Sealy, and D. Bronson, "A high efficiency 5 kw inductive charger for EVs using dual side control," *IEEE Trans. Ind. Informat.*, vol. 8, no. 3, pp. 585–595, Aug. 2012.

[2] C.-H. Ou, H. Liang, and W. Zhuang, "Investigating wireless charging and mobility of electric vehicles on electricity market," *IEEE Trans. Ind. Electron.*, vol. 62, no. 5, pp. 3123–3133, May 2015.

[3] A. K. Swain, S. Devarakonda, and U. K. Madawala, "Modeling, sensitivity analysis, and controller synthesis of multipickup bidirectional inductive power transfer systems," *IEEE Trans. Ind. Informat.*, vol. 10, no. 2, pp. 1372–1380, May 2014.

[4] J. Kim, D.-H. Kim, J. Choi, K.-H. Kim, and Y.-J. Park, "Free-positioning wireless charging system for small electronic devices using a bowl-shaped transmitting coil," *IEEE Trans. Microw. Theory Tech.*, vol. 63, no. 3, pp. 791–800, Mar. 2015.

[5] M. Fu, T. Zhang, X. Zhu, P. C.-K. Luk, and C. Ma, "Compensation of cross coupling in multiple-receiver wireless power transfer systems," *IEEE Trans. Ind. Informat.*, vol. 12, no. 2, pp. 474–482, Apr. 2016.

[6] M. Fu, C. Ma, and X. Zhu, "A cascaded boost-buck converter for high efficiency wireless power transfer systems," *IEEE Trans. Ind. Inform.*, vol. 10, no. 3, pp. 1972–1980, July 2015.

[7] P. S. Riehl, A. Satyamoorthy, H. Akram, Y.-C. Yen, J.-C. Yang, B. Juan, C.-M. Lee, F.-C. Lin, V. Muratov, W. Plumb *et al.*, "Wireless power systems for mobile devices supporting inductive and resonant operating modes," *IEEE Trans. Microw. Theory Tech.*, vol. 63, no. 3, pp. 780–790, Mar. 2015.

[8] M. Fu, H. Yin, M. Liu, and C. Ma, "Loading and power control for a high-efficiency class E PA-driven megahertz WPT system," *IEEE Trans. Ind. Electron.*, vol. 63, no. 11, pp. 6867–6876, Nov. 2016.

[9] S. Aldhaher, D. C. Yates, and P. D. Mitcheson, "Design and development of a class EF2 inverter and rectifier for multi-megahertz wireless power transfer systems," *IEEE Trans. Power Electron.*, vol. 31, no. 12, pp. 8138–8150, Feb. 2016.

[10] C. Wang, G. A. Covic, and O. H. Stielau, "Power transfer capability and bifurcation phenomena of loosely coupled inductive power transfer systems," *IEEE Trans. Ind. Electron.*, vol. 51, no. 1, pp. 148–157, Feb. 2004.

[11] J. Salln, J. L. Villa, A. Llombart, and J. F. Sanz, "Optimal design of ICPT systems applied to electric vehicle battery charge," *IEEE Trans. Ind. Electron.*, vol. 56, no. 6, pp. 2140–2149, June 2009.

[12] W. Zhang, S.-C. Wong, C. Tse, and Q. Chen, "Design for efficiency optimization and voltage controllability of series-series compensated inductive power transfer systems," *IEEE Trans. Power Electron.*, vol. 29, no. 1, pp. 191–200, Jan. 2014.

[13] Y. H. Sohn, B. H. Choi, E. S. Lee, G. C. Lim, G.-H. Cho, and C. T. Rim, "General unified analyses of two-capacitor inductive power transfer systems: Equivalence of current-source ss and sp compensations," *IEEE Trans. Power Electron.*, vol. 30, no. 11, pp. 6030–6045, Nov. 2015.

[14] Z. Pantic, S. Bai, and S. M. Lukic, "ZCS LCC-compensated resonant inverter for inductive-power-transfer application," *IEEE Trans. Ind. Electron.*, vol. 58, no. 5, pp. 3500–3510, Aug. 2011.

[15] J. Kim, D.-H. Kim, and Y.-J. Park, "Analysis of capacitive impedance matching networks for simultaneous wireless power transfer to multiple devices," *IEEE Trans. Ind. Electron.*, vol. 62, no. 5, pp. 2807–2813, May 2015.

[16] S. Kong, B. Bae, D. H. Jung, J. J. Kim, S. Kim, C. Song, J. Kim, and J. Kim, "An investigation of electromagnetic radiated emission and interference from multi-coil wireless power transfer systems using resonant magnetic field coupling," *IEEE Trans. Microw. Theory Tech.*, vol. 63, no. 3, pp. 833–846, Mar. 2015.

[17] M. Dionigi, M. Mongiardo, and R. Perfetti, "Rigorous network and full-wave electromagnetic modeling of wireless power transfer links," *IEEE Trans. Microw. Theory Tech.*, vol. 63, no. 1, pp. 65–75, Jan. 2015.

[18] S. Aldhaher, P. C. K. Luk, K. E. K. Drissi, and J. Whidborne, "High-input-voltage high-frequency class E rectifiers for resonant inductive links," *IEEE Trans. Power Electron.*, vol. 30, no. 3, pp. 1328 – 1335, Mar. 2015.
[19] M. Liu, M. Fu, and C. Ma, "Parameter design for a 6.78 MHz wireless power transfer system based on analytical derivation of class E current-driven rectifier," *IEEE Trans. Power Electron.*, vol. 31, no. 6, pp. 4280–4291, June 2016.
[20] J.-H. Choi, S.-K. Yeo, S. Park, J.-S. Lee, and G.-H. Cho, "Resonant regulating rectifiers (3R) operating for 6.78 MHz resonant transfer (RWPT)," *IEEE J. Solid-State Circuits*, vol. 48, no. 12, pp. 2989–3001, Dec. 2013.
[21] Y. Lu and W.-H. Ki, "A 13.56 MHz CMOS active rectifier with switched-offset and compensated biasing for biomedical wireless power transfer systems," *IEEE Trans. Biomed. Circuits Syst.*, vol. 8, no. 3, pp. 334–344, June 2014.
[22] M. K. Kazimierczuk and D. Czarkowski, *Resonant power converters*. John Wiley & Sons, 2012.
[23] M. Fu, H. Yin, X. Zhu, and C. Ma, "Analysis and tracking of optimal load in wireless power transfer systems," *IEEE Trans. Power Electron.*, vol. 30, no. 7, pp. 3952–3963, July 2015.
[24] M. Fu, Z. Tang, M. Liu, C. Ma, and X. Zhu, "Full-bridge rectifier input reactance compensation in megahertz wireless power transfer systems," in *IEEE PELS Workshop on Emerging Technologies: Wireless Power (WoW)*, Daejeon, Korea, June 2015, pp. 1–5.
[25] Z. Tang, M. Fu, M. Liu, and C. Ma, "Optimization of the compensation capacitors for megahertz wireless power transfer systems," in *the 41st Annual Conference of the IEEE Industrial Electronics Society*, Yokohama, Japan, Nov. 2015, pp. 1447–1452.
[26] K. Chen, Z. Zhao, L. Yuan, T. Lu, and F. He, "The impact of nonlinear junction capacitance on switching transient and its modeling for SiC MOSFET," *IEEE Trans. Electron Devices*, vol. 62, no. 2, pp. 333–338, Feb. 2015.
[27] T. Funaki, T. Kimoto, and T. Hikihara, "Evaluation of high frequency switching capability of SiC schottky barrier diode, based on junction capacitance model," *IEEE Trans. Power Electron.*, vol. 23, no. 5, pp. 2602–2611, Sep. 2008.
[28] R. Fu, A. E. Grekov, K. Peng, and E. Santi, "Parameter extraction procedure for a physics-based power SiC schottky diode model," *IEEE Trans. Ind. Appl.*, vol. 50, no. 5, pp. 3558–3568, Sep. 2014.
[29] T. C. Beh, M. Kato, T. Imura, S. Oh, and Y. Hori, "Automated impedance matching system for robust wireless power transfer via magnetic resonance coupling," *IEEE Trans. Ind. Electron.*, vol. 60, no. 9, pp. 3689–3698, Sep. 2013.
[30] M. J. Neath, A. K. Swain, U. K. Madawala, and D. J. Thrimawithana, "An optimal PID controller for a bidirectional inductive power transfer system using multiobjective genetic algorithm," *IEEE Trans. Power Electron.*, vol. 29, no. 3, pp. 1523–1531, Mar. 2014.

Minfan Fu (S'13-M'16) received the B.S., M.S., and Ph.D. degrees in electrical and computer engineering from University of Michigan-Shanghai Jiao Tong University Joint Institute, Shanghai Jiao Tong University, Shanghai, China in 2010, 2013, and 2016, respectively.

He is currently an Assistant Professor at the School of Information Sceience and Technology (SIST), ShanghaiTech University, Shanghai, China. Between 2016 and 2018, he held a postdoctoral position with the Center for Power Electronics Systems (CPES), Virginia Polytechnic Institute and State University, Blacksburg, VA, USA. His research interests include megahertz wireless power transfer, high-frequency power conversion, high-frequency magnetic design, and application of wide-band-gap devices.

Zefan Tang (S'15-M'18) received the B.S. degree in mechanical engineering from Zhejiang University, Zhejiang, China, in 2014, and the M.S. degree in electrical and computer engineering from the University of Michigan-Shanghai Jiao Tong University Joint Institute, Shanghai Jiao Tong University, Shanghai, China, in 2017.

He is currently working toward the Ph.D. degree in electrical engineering with the University of Connecticut, Storrs, CT, USA. His current research interests include distributed renewable energy systems, power system resilience, cyber security, machine learning, and extreme value analysis.

Chengbin Ma (M'05-SM'18) received the B.S. (Hons.) degree in industrial automation from East China University of Science and Technology, Shanghai, China, in 1997, and the M.S. and Ph.D. degrees both in electrical engineering from The University of Tokyo, Tokyo, Japan, in 2001 and 2004, respectively.

He is currently an Associate Professor of electrical and computer engineering at University of Michigan-Shanghai Jiao Tong University Joint Institute, Shanghai Jiao Tong University, Shanghai, China. Between 2006 and 2008, he held a postdoctoral position with the Department of Mechanical and Aeronautical Engineering, University of California Davis, California, USA. From 2004 to 2006, he was an R&D researcher with Servo Laboratory, Fanuc Limited, Yamanashi, Japan. His research interests include energy management, megahertz wireless power transfer, dynamics and motion control, and wide applications in electronic devices, electric vehicles, microgrids and smart grids, etc.

Prof. Ma is an Associate Editor for the IEEE Transactions on Industrial Informatics.